Dry and Direct Deposition of Aerosol Synthesized Single-Walled Carbon Nanotubes by Thermophoresis

Patrik Laiho[a], Kimmo Mustonen[a,b], Yutaka Ohno[c], Shigeo Maruyama[d], Esko I. Kauppinen[a*]*

[a] Department of Applied Physics, Aalto University School of Science, P.O. Box 15100, FI-00076 Aalto, Finland

[b] Physics of Nanostructured Materials, Faculty of Physics, University of Vienna, Boltzmanngasse 5, A-1090 Vienna, Austria

[c] Institute of Materials and Systems for Sustainability, Nagoya University, Furo-cho, Chikusa-ku, Nagoya 464-8603, Japan

[d] Department of Mechanical Engineering, The University of Tokyo, Bunkyo-ku, Tokyo 113-8656, Japan

[*] Correspondence should be addressed to: patrik.laiho@aalto.fi, esko.kauppinen@aalto.fi

KEYWORDS: aerosol technology; aerosol deposition; thermophoresis; single-walled carbon nanotubes; floating catalyst chemical vapor deposition; thin film transistors

Introduction and Abstract

Single-walled carbon nanotubes (SWCNTs) show great potential as an active material in electronic and photonic devices, but their applicability is currently limited by shortcomings in existing deposition methods. SWCNTs can be dispersed from liquid solutions, however, their poor solubility requires the use of surfactants and ultrasonication, causing defects and degradation in device performance. Likewise, the high temperatures required by their chemical vapor deposition growth limit substrates on which SWCNTs can be directly grown. Here, we present a systematic study of the direct deposition of pristine, aerosol-synthesized SWCNTs by thermophoresis. The density of the deposited nanotube film can be continuously adjusted from individual, separated nanotubes to multilayer thin films by changing the deposition time. Depending on the lateral flow inside the thermophoretic precipitator, the angular distribution of the deposited SWCNT film can be changed from uniform to non-uniform. Since the substrate is kept at nearly ambient temperature, deposition can be thus carried out on practically any flat substrate with high efficiencies close to unity. The thermophoretic terminal velocity of SWCNTs, determined by aerosol loss measurements, is found to be approximately one third of the usual prediction in the free molecular regime and shows a weak dependence on the nanotube diameter. As a demonstration of the applicability of our technique, we have used thermophoretic deposition in the fabrication of carbon nanotube thin film transistors with uniform electrical properties and a high, over 99.5%, yield.

Thin films of single-walled carbon nanotubes (SWCNTs) show great potential in a range of applications, such as transparent conductive electrodes[1], thin film transistor channels[2], and saturable absorbers[3]. Likewise, individual semiconducting SWCNTs[4] and aligned arrays[5] of them are a promising building block for nanoscale electronics[6-7], and suspended SWCNTs have potential applications in nanoelectromechanical components[8]. While random and aligned[9] SWCNTs can be grown directly on substrates from catalyst particles or stripes using chemical vapor deposition (CVD), this can be only carried out on substrates that can withstand the high temperatures involved (typically 700-1000°C). Alternatively, the SWCNTs must be transferred to a target substrate[10] or dispersed in a solution. SWCNTs can be deposited from solution by dropcasting[11], printing[12], or the Langmuir-Blodgett[13] and Langmuir-Schaefer[14] methods for example, but their dispersion by surfactants and ultrasonication adversely modifies their electronic properties due to surfactant remains and sonication-induced lattice defects[15] and cutting[16].

Previously, we have demonstrated that thin films of aerosol-synthesized SWCNTs, collected by a dry and dispersion-free filtration process, can be used as high-performance transparent conducting electrodes[17] and thin film transistor (TFT) channels[18]. However, this method is limited by the size of the filter, and dry press transfer[17] of the films is reliable only when the film is thick enough to form a continuous, interlocking structure. Sparser films close to the percolation threshold and suitable for TFT fabrication can be transferred by dissolving the filter[18], but the dissolution is time-consuming, may contaminate the substrate and compromises the otherwise solvent-free process. In either case, reliable deposition of separated, individual SWCNTs cannot be carried out.

Here, we have for the first time systematically studied the direct deposition of SWCNT aerosols by thermophoresis. In general, thermophoretic deposition of aerosol nanoparticles is a promising method for the fabrication of nanoparticle thin films and coatings[19] and catalyst preparation for chemical vapor deposition (CVD) growth processes on surfaces[20,21]. Thermophoretic precipitators (TP) can be designed so that the deposition efficiency can almost reach unity and the substrate can be kept at near-ambient conditions, meaning that deposition can be carried out on practically any flat substrate, including mechanically or chemically sensitive materials and flexible polymers.

Usually, the size of engineered nanoparticles and nanoparticle agglomerates ranges from a few to tens of nanometers, indicating that their thermophoresis occurs in the free molecular regime. Assuming rigid body collisions between the surrounding gas molecules and the particle surface, Waldmann *et al*[22-23]. determined that the thermophoretic terminal velocity v_{th} in the free molecular regime, obtained by balancing the Stokes drag force and the thermophoretic force ($F_D + F_{th} = 0$), is

$$v_{th} = -\frac{\kappa \nabla \mathrm{T}}{5\left(1+\frac{\pi\varphi}{8}\right)NkT} = -\frac{3\mu_g \nabla \mathrm{T}}{4\left(1+\frac{\pi\varphi}{8}\right)\rho_g T}, \qquad [1]$$

where $\kappa = 15k\mu_g/4m_g$ is the temperature conductivity of the gas[24], φ is the momentum accommodation factor, describing the proportion of specular and diffusive scattering on the particle surface and normally assumed to be 0.9 based on experiments[25], N is the number density of the gas, k is Boltzmann's constant, μ_g is the viscosity of the gas, $\rho_g = Nm_g$ is the mass density

of the gas and m_g is the mass of the gas molecule. Since the terminal velocity predicted by Eq. 1 is independent of the particle size and composition, thermophoretic sampling is also attractive in the sense that non-biased size distributions can be measured from deposited samples.

The dependence of v_{th} on the shape of non-spherical particles in the free molecular regime has been considered theoretically by Rosner *et al.*[26], concluding that the v_{th} of sphero-cylindrical particles and random, chain-like agglomerates of spherical particles is nearly equal to that of equal volume spherical particles when the particles are randomly oriented, and differ slightly when the particle is aligned perpendicular or parallel to the temperature gradient. In the case of purely specular collisions, Zurita-Gotor has concluded[27] that v_{th} is exactly independent of size and structure and equivalent to the prediction of Eq. 1, indicating that size distributions measured from thermophoretically sampled non-spherical particles should also be nonbiased.

The high aspect ratios of SWCNTs, and the fact that their cross section is molecular in scale while the length is typically on the order of micrometers, complicates their description in terms of aerosol theory. We have previously determined that their electrical mobility diameters d_{ME} range from tens of nanometers for non-agglomerated SWCNTs[28] to ca. 100 nm for agglomerated SWCNTs[29]. Likewise, we have shown[30] that the diffusive agglomeration rate of individual SWCNTs with a mean length of 3 μm, a mean diameter of 1 nm, and a mean d_{ME} of 36 nm can be predicted by using a mobility diameter of 20 nm. Here, we have measured the deposition rates of SWCNTs with various mean diameters using aerosol loss measurements and compared them with theory and the experimental deposition rate of a near-spherical iron nano-agglomerate aerosol obeying Eq. 1. We have found that the thermophoretic terminal velocity differs from the

prediction of Eq. 1 and depends weakly on the mean SWCNT diameter. We suggest that this behavior is mainly caused by the invalidity of the assumption of rigid body collisions behind Eq. 1 and possibly by additional mechanisms discussed here. Centimeter-scale thin films with uniform spatial densities can be deposited even with a simple plate-to-plate TP, and the SWCNTs can be aligned to a limited extent using shear flow during the deposition. The applicability of the method is also demonstrated by the fabrication of an array of thin film transistors using the TP.

Thermophoretic deposition can also be used to deposit SWCNTs on prefabricated micro- and nanostructures without damaging them, to guide synthesis process development by providing nonbiased SWCNT size distributions, and could be used to fabricate van der Waals heterostructures consisting of SWCNTs and such two-dimensional solids as graphene, hexagonal boron nitride, or transition metal dichalcogenides[31] without solution processing. Our findings can also be useful when considering thermophoretic losses in the design of aerosol CVD reactors and when evaluating human exposure to airborne aerosolized SWCNTs.

Results and discussion

We studied the deposition of SWCNTs with three different mean diameters (d = 1.2 nm, d = 1.5 nm, d = 1.9 nm), grown using the floating catalyst CVD process with ferrocene as the catalyst source, carbon monoxide (CO) as the carbon feedstock, and carbon dioxide (CO_2) to control the SWCNT mean diameter. This process is known to yield a mixture of semiconducting and metallic single-walled carbon nanotubes with the semiconducting-to-metallic ratio close to the expected value of 2:1, and with a preference towards near-armchair chiralities[28]. Because

carbon monoxide does not undergo thermal self-decomposition at the reaction conditions, the synthesized SWCNTs are not contaminated by amorphous carbon or other carbonaceous side products. The mean diameters of the SWCNTs were determined by UV/Vis/NIR absorbance of thin film samples collected by filtration and measuring the positions of the absorption peaks assigned to the first and second electronic transitions of semiconducting SWCNTs (S_{11} and S_{22}). The first electronic transition of metallic SWCNTs (M_{11}) was also observed, indicating their presence. For comparison, we also studied the deposition of an aerosol consisting of near-spherical nanoscale agglomerates of iron nanoparticles with a similar electrical mobility diameter, produced using a spark discharge generator[28]. Schematics of the synthesis equipment are presented in Figure 1a and Figure 1b. During synthesis, the number concentration at the outlet of the CVD reactor was at or below $10^6/cm^3$ by adjusting the catalyst precursor feed to prevent excessive SWCNT agglomeration. At this concentration, the process is expected to yield predominantly individual SWCNTs and small bundles with diameters below 2 nm.[32]

A purpose-built modular plate-to-plate TP was used in this work. The TP consists of two aluminum plates separated by a polytetrafluoroethylene (PTFE) plate, in which a rectangular flow channel has been cut. The substrate is based on the lower plate in a rectangular, 0.5 mm deep recession and is surrounded by a smaller PTFE plate with a hole in the shape and size of the substrate and a matching thickness, so that the substrate and the top surface of the smaller PTFE plate form the bottom of the flow channel. The top plate is heated using two power resistors and a tabletop voltage source (maximum heating power 84 W), and the bottom plate is cooled by ambient temperature water cooling. Due to the low thermal conductivity of the PTFE plate separating the hot and cold plate, at full heating power a temperature gradient of ca. 10^5 Km^{-1}, estimated as the temperature difference of the hot and cold plate divided by the height of the

upper PTFE plate, can be reached in the 0.25 or 0.5 mm high channel. The aerosol enters and exits the channel through the upper plate through two 1/4 inch pipes. 500 μm thick Si/SiO_2 chips (100 nm thermal oxide on one side) with lateral dimensions of approximately 1.5 x 1.5 cm were used as the deposition substrate. A schematic of the TP is presented in Figure 1c. Deposition of SWCNTs on other substrates was also carried out; micrographs of deposited SWCNTs are included in the Supporting Information. The optical absorbance spectra of the SWCNTs, measured from thin film samples collected by filtration and transferred on quartz by pressing, used to determine their mean diameters, are presented in Figure 1d.

Before deposition, the number size distributions of the SWCNT aerosols were measured to ensure that the reactor was not producing a significant amount of inactive catalyst nanoparticles. The measured aerosol number size distributions, presented in Figure 1e, were comparable to earlier published distributions[28,32] with mean d_{ME} at 40-60 nm. The parameters of the spark discharge generator were adjusted so that the number size distribution of the Fe agglomerates approximately matched the SWCNT number size distributions.

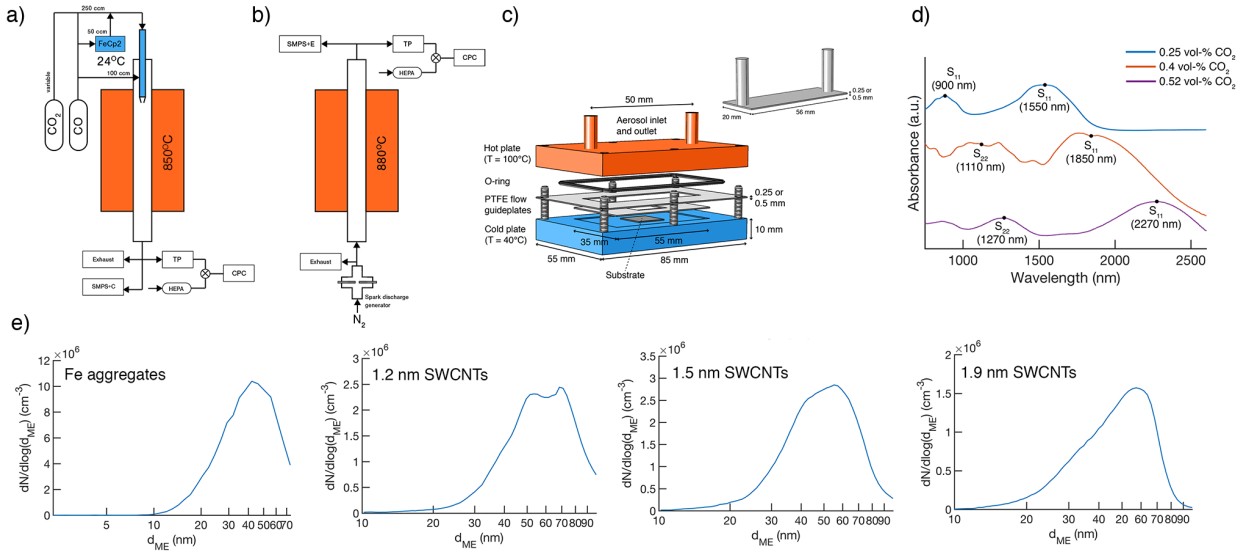

Figure 1. Schematics of the synthesis and deposition systems, SWCNT optical absorption spectra and electrical mobility distributions. **a)** Schematic representation of the SWCNT growth system. **b)** Schematic representation of the iron nano-agglomerate growth system. **c)** Schematic representation of the plate-to-plate thermophoretic precipitator and the flow channel defined by the plates and the cut in the upper PTFE plate (inset). **d)** UV/Vis/NIR absorption spectra of the synthesized SWCNTs. The means of the peaks assigned to the semiconducting S_{11} and S_{22} electronic transitions, used to determine the mean SWCNT diameters, are indicated. **e)** Number size distributions of the Fe nano-agglomerates and SWCNTs.

The relative aerosol loss in the TP channel, corresponding to its collection efficiency, as a function of the temperature gradient was studied by pumping either iron nano-agglomerate or SWCNT aerosol with variable volume flow rates through the TP and simultaneously measuring the aerosol number concentration and the temperature gradient during a full heating and cooling cycle. A logging interval of ten seconds was used for both measurements. Representative measurements of the temperature gradient and aerosol number concentration are presented in Figure 2a. The relative loss in the precipitator was calculated as

$$\eta_{exp} = 1 - \frac{C(dT)}{C(dT=0)}, \qquad [2]$$

where the baseline concentration $C(dT = 0)$ was measured through an unheated TP to account for possible non-thermophoretic losses, such as diffusive and impaction losses, in the sampling lines and depositor entries.

Assuming that the aerosol in the channel spreads quickly to a spatially uniform distribution after the inlet, the efficiency for a given set of channel dimensions and volume flow rate can be predicted from

$$\eta_{th} = \min\left(1, \frac{\overline{v_{th}} t_{res,x}}{h}\right), \qquad [3]$$

where $\overline{v_{th}}$ is the average terminal velocity in the channel, and $t_{res,x} = {}^{l}/_{Qwh}$, where Q is the volume flow rate, and w and h are the width and height of the channel. The average terminal velocity $\overline{v_{th}}$ was evaluated by assuming that the temperature profile is linear in the z direction and evaluating $v_{th}(z)$ by Eq. 1, using $\nabla T = \frac{T_{hot} - T_{cold}}{h}$ as the temperature gradient and the average of T_{hot} and T_{cold} as T, and calculating the gas viscosity μ from

$$\frac{\mu}{\mu_0} = \frac{T_0 + T_s}{T + T_s}\left(\frac{T}{T_0}\right)^{3/2}, \qquad [4]$$

where T_s is Sutherland's constant (240 for CO and 111 for N_2)[33] , and μ_0 and T_0 are the reference viscosity and temperature (1.76×10^{-5} Pas and 298 K for CO, 1.781×10^{-5} Pas and 300.55 K for N_2) and the gas density from $\rho = \rho_{ref}T_{ref}/T$, where ρ_{ref} and T_{ref} are a reference density and temperature (1.165 kgm^{-3} and 293 K for both N_2 and CO)[34]. Due to the low volume fraction (less than one volume percent introduced and a trace amount produced by CO disproportionation during the SWCNT growth) of CO_2, the carrier gas of the SWCNTs was assumed to be purely CO.

We measured the deposition efficiency of the iron nano-agglomerates and three different populations of predominantly non-bundled SWCNTs using six different combinations of channel geometry and flow rate. The deposition rate of the iron nano-agglomerates was close to the prediction calculated using Eq. 1, as expected based on the size distribution of the aerosol. A slight deviation from the prediction was observed at > 8×10^4 Km^{-1}, where the predicted efficiency approaches unity. This could be a result of a number of non-idealities in the model and the experimental setup: the underlying assumption of a uniform vertical distribution of the aerosol may not hold entirely, the flow channel used in the experiments can be slightly irregular in shape, or the deposition of some particles is prevented by local eddies lifting them away from the surface. Meanwhile, we found the deposition rate of the SWCNT aerosol was systematically lower and also slightly affected by the nanotube mean diameter. Increasing the diameter from 1.2 nm to 1.5 nm and finally to 1.9 nm resulted in respective deposition rates of 35%, 39% and 43% of the prediction of Eq. 1. The full set of six measurements per each aerosol material is included in the Supporting Information.

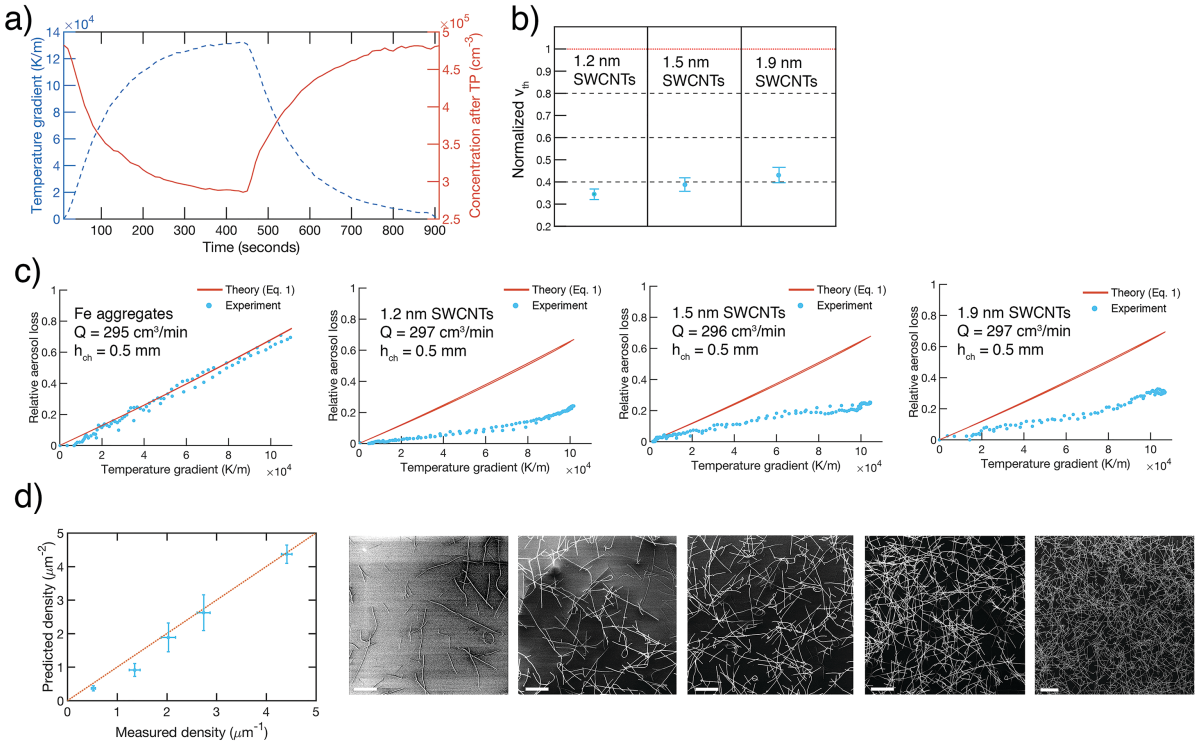

Figure 2. Measurements of aerosol deposition efficiency. **a)** Representative real-time measurement of the aerosol concentration (1.2 nm SWCNTs, h_{ch} = 0.25 mm, Q = 208 cm^3/min) passed through the precipitator and the temperature gradient between the precipitator plates. The heating is started at t = 0 seconds and turned off at t = 450 seconds. **b)** The measured mean deposition efficiencies for each type of SWCNT aerosol, expressed as a fraction of the theoretical prediction based on Eq. 1. The error bars indicate one standard deviation. **c)** Representative deposition efficiency versus temperature gradient measurements for Fe agglomerates and SWCNTs. The red solid line indicates the predicted density based on Eq. 1., and the blue circles indicate experimental data. **d)** Predicted versus measured SWCNT density (scale bars 2 μm in all micrographs). The vertical error bars indicate experimental error, arising mainly from shift in aerosol concentration during the deposition. The horizontal error bars indicate one standard deviation. The red dashed line is to guide the eye.

The discrepancy between the observed deposition rates and Eq. 1 may arise due to several different previously published mechanisms. As the particle size is reduced to the molecular scale, the assumptions of a constant momentum accommodation factor and rigid body collisions are no longer expected to be accurate due to intermolecular forces between the particle surface and gas molecules. Li and Wang have proposed modified forms for the drag[35] and thermophoretic[36] forces, resulting in

$$v_{th} = \left(1 - \frac{6}{5}\frac{\Omega_{avg}^{(1,2)*}}{\Omega_{avg}^{(1,1)*}}\right)\frac{\kappa \nabla \mathrm{T}}{NkT} = \left(1 - \frac{6}{5}\frac{\Omega_{avg}^{(1,2)*}}{\Omega_{avg}^{(1,1)*}}\right)\frac{15\mu_g \nabla \mathrm{T}}{4\rho_g T}, [5]$$

where the reduced collisions integrals $\Omega_{avg}^{(1,l)*}$ describe the intermolecular forces, averaged over diffuse and specular scattering, between the gas molecules ($l = 1$), and between the gas molecules and the particle surface ($l = 2$). At particle diameters below 5 nm, the predicted terminal velocities of Eqs. 1 and 5 may even differ by orders of magnitude.

A diameter dependence similar to the one observed experimentally, although with less diminished deposition rates of 53%, 65% and 77% at 1.2 nm, 1.5 nm, and 1.9 nm, is predicted by Eq. 5. A plot of the terminal velocity predicted by Eq. 5 as a function of the particle diameter, calculated using elemental carbon as the particle material and CO as the gas molecule, is included in the Supporting Information. During the review of our work, a recently published work by Wang *et al.*, specifically considering the thermophoresis of nanocylinders came to our attention[37]. The authors of the paper extend the earlier results of Li and Wang, and the quantitative results they obtain are close to the values we have obtained. It can also be assumed that the SWCNTs are at least partly oriented perpendicularly to the temperature gradient during

deposition by the surrounding flow, which may further contribute to the discrepancy. The effect of such an alignment on the thermophoresis of non-spherical particles has been considered by Rosner *et al.*[26], but the two cases (sphero-cylindrical particles in the free molecular regime and chain-like agglomerates in the continuum regime) and aspect ratios covered (L/2R up to 100) do not match the dimensions of the SWCNTs measured in our study. Nevertheless, their results indicate that alignment may contribute to the diminishing of the terminal velocity.

Due to the micrometer-scale length of SWCNTs and their and high thermal conductivity, up to 3500 W m^{-1} K^{-1} at room temperature[38], the terminal velocity could in principle be further diminished because the temperature gradient is disturbed by thermal conduction along the SWCNT axis. A semi-empirical model, accounting for this effect and describing thermophoresis in the transition regime between the free molecular and continuum regimes, has been proposed by Talbot *et al.*[39] and found to match experimental deposition rates measured in laminar and turbulent pipe flows using monodisperse NaCl particles[40].

Since the model of Talbot *et al.* is expressed in terms of the Knudsen number $Kn = 2\lambda/d_p$, a quantitative prediction cannot be obtained for SWCNTs without assuming some effective size for d_p. However, since the terminal velocity is predicted to decrease rapidly with a decreasing *Kn* when k_g/k_p is small (corresponding to particles with high thermal conductivities; $k_{CO}/k_{SWCNT} \sim 7\times10^{-6}$), this mechanism is also a possible cause for the observed decreased terminal velocities. A comparison of terminal velocities predicted by Eq. 1 and the model of Talbot *et al.* as a function of Kn is included in the Supporting Information. We suggest that the mechanisms underlying thermophoresis of SWCNT aerosols could be studied in the future using SWCNTs with significantly shorter or longer mean lengths and similar diameters, or SWCNTs with

significantly larger diameters than the ones considered here. Study of the deposition efficiencies of such SWCNTs, when they become available by developments of the floating catalyst CVD method, could differentiate more clearly between the suggested mechanisms.

The collection efficiency of the TP was also evaluated by comparing the area density of deposited 1.2 nm SWCNTs measured from scanning electron (SEM) micrographs against the prediction

$$\rho = \frac{\eta_{th} Q C t}{A}, \qquad [7]$$

where η_{th} is the efficiency of the TP at a given temperature gradient and flow rate, extrapolated from the measured efficiencies, Q is the volume flow through the TP, C is the SWCNT concentration measured using a condensation particle counter (CPC), t is the collection time and A is the lateral area of the channel. The predicted and measured SWCNT densities were found to match well, as presented in Figure 2d. To facilitate the measurement, the area density (um^{-2}) was approximated by the linear density (um^{-1}), measured by detecting peaks in the grey values of the SEM scanlines. An example of an analyzed scanline is presented in Figure 4b.

The length and orientation distributions of the deposited SWCNTs were analyzed using FiberApp, an open-source software for tracking and measuring fibrous objects[41]. The length distributions of the three SWCNT populations, used to study the deposition efficiency, were measured from several SEM micrographs, similar to those presented in Figure 3a. We found that the measured distributions for all studied synthesis conditions, presented in Figure 3b, were log-

normal to a high precision in the range of 0.5 to 15 μm, as expected of aerosol-synthesized SWCNTs, implying that the sampling method does not introduce a strong bias based on SWCNT length.

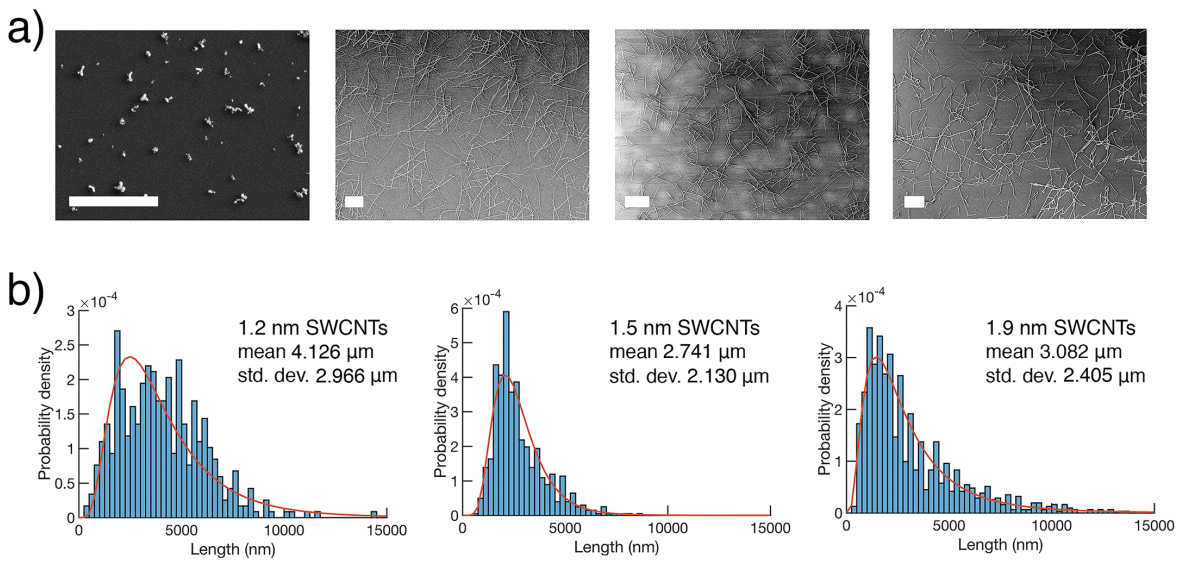

Figure 3. SEM analysis of the deposited Fe agglomerates and SWCNTs. **a)** Representative SEM micrographs of deposited Fe agglomerates (scale bar 1 μm) and SWCNTs (scale bars 2 μm) **b)** Length statistics measured from deposited SWCNTs. The red curves show log-normal maximum likelihood fits ($\mu = 8.16$, $\sigma = 0.58$ for 1.2 nm SWCNTs, $\mu = 7.82$, $\sigma = 0.43$ for 1.5 nm SWCNTs, and $\mu = 7.78$, $\sigma = 0.71$ for 1.9 nm SWCNTs) on the data.

The uniformity of the deposited SWCNT film was evaluated from nine SEM micrographs obtained at the center and edges of a 1 cm^2 square, depicted in Figure 4a. When deposition was carried out using a volume flow of 80 cm^3/min through a 0.5 mm x 2 cm x 5 cm channel, a film with high spatial uniformity over an area of 1 x 1 cm was obtained and no preferential alignment of the SWCNTs was observed. Deposition using a higher flow rate of 300 cm^3/min through a

channel with identical dimensions resulted in a non-uniform spatial density, with comparably fewer nanotubes along the centerline of the measured area. Increasing the flow rate also resulted in a non-uniform angular distribution, showing preferential alignment with the flow direction (corresponding to an angle of 0 in the histograms and the vertical axis in the micrographs). The spatial density distribution, expressed in terms of the SWCNT linear densities per scanline, and the angular distribution of the SWCNTs in each of the micrographs, are presented in Figs. 4c and 4d. The alignment was quantified using the 2D order parameter

$$S_{2D} = 2\langle \cos^2 \theta_n \rangle - 1, \qquad [8]$$

where the brackets indicate the mean over *n* fiber segments and θ_n is the angle between the *n*th segment and the average orientation of the population. The order parameters measured from the sample collected at a flow rate of 100 cm^3/min were close to zero, indicating a random distribution, whereas values of S_{2D} = 0.2345, 0.2493, and 0.2685 was observed at the centerline of the sample collected at 300 cm^3/min. We believe that a higher flow velocity in the center of the channel results in a higher shear rate, increasing the alignment, while simultaneously decreasing the residence time and deposition efficiency of the SWCNTs.

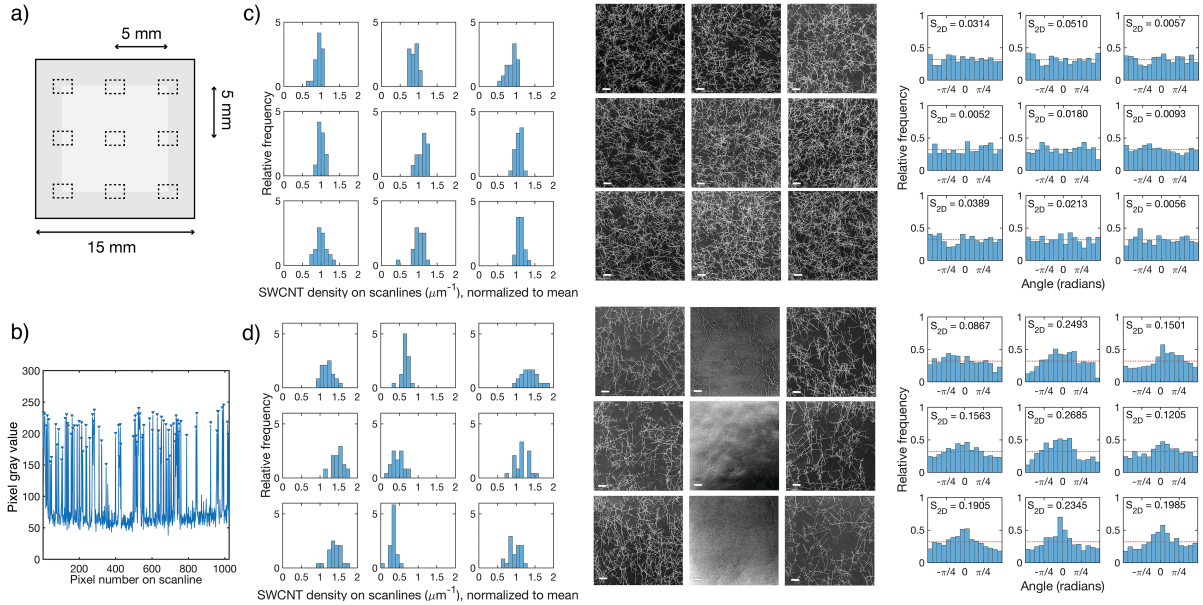

Figure 4. Spatial and angular uniformity of the deposited SWCNTs. a) Schematic (not to scale) of the micrograph locations on the sample. The light grey area depicts the middle 1 cm^2 of the sample. b) A representative analyzed SEM scanline, with assigned SWCNT locations indicated by triangles. c) and d) Spatial density distribution, representative micrographs obtained at nine points depicted in a) (scale bars: 1 μm) and angular distributions (the horizontal red line indicates a uniform distribution) of films deposited using flows of c) 80, and d) 300 cm^3/min. The densities are normalized to means of 2.18 μm^{-1} and 1.18 μm^{-1}, for 80 cm^3/min and 300 cm^3/min deposition flows, respectively).

To demonstrate the applicability of the thermophoretically deposited SWCNTs as a functional coating, SWCNT thin film transistors were fabricated from the d = 1.2 nm SWCNTs using a process similar to one employed earlier using filter-transferred SWCNT networks[18,32, 42]. The d = 1.2 nm population was chosen to keep the results comparable with the earlier studies, carried out using SWCNTs with nearly similar diameters. The TFTs used a common back-gate design with

100 nm thermal silicon oxide as the dielectric, Ti/Au (5 nm, 40 nm) source and drain electrodes deposited using electron beam evaporation and the non-oxidized reverse of the chip, on which a Al contact was sputtered, as the gate electrode. The SWCNTs were thermophoretically deposited on prefabricated arrays of source and drain electrodes and the channel areas were defined by reactive ion etching using an oxygen and argon plasma. The test structure used in the work contained channels with widths of 100, 200 and 500 μm and lengths of 5, 10, 20, 30, 40, 50, and 100 μm.

Device characterization was carried out in ambient conditions on a semi-automatic probe station (PA200, Süss MicroTec AG) connected to a semiconductor parameter analyzer (Agilent 4156). The transfer characteristics were measured using a source-drain bias of -1 V and a double gate voltage sweep from -10 to 10 V.

The field-effect device mobilities of the devices were evaluated using the standard formula

$$\mu = \frac{L_{CH}}{W_{CH}} \frac{1}{V_{DS}} \frac{1}{C} \frac{dI_D}{dV_{GS}}, \qquad [9]$$

where L_{CH} and W_{CH} are the length and width of the channel, V_{DS} is the source-drain voltage, C is the channel capacitance and dI_D/dV_{GS} is the maximum of the transconductance. The channel capacitance was evaluated using the model of Cao *et al.*, accounting for the electric field focusing on a sparse SWCNT network[43]:

$$C = D/\left[C_Q^{-1} + (2\pi\varepsilon_0\varepsilon_s)^{-1} \log\left(\frac{\sinh(2\pi t D)}{\pi R D}\right)\right], \qquad [10]$$

where D is the linear SWCNT density (0.96 SWCNTs/μm based on SEM of the finished devices), $C_Q = e^2 g_0 \approx 3.2$ is the quantum capacitance, R is the mean radius of the SWCNT, t is the dielectric thickness, and ε_s is the relative permittivity of the dielectric.

Transfer and output characteristics and micrographs of a finished device are presented in Figure 5. The transfer curves of all measured devices are included in the Supporting Information. Based on an evaluation of the ON state (V_{GS} = -10 V) resistances of 100 μm wide devices as a function of the channel length, the total resistance of the device is dominated by the resistance of the relatively sparse SWCNT network, as can be expected. The fabricated thin film transistors exhibited uniform electrical properties across the centimeter-sized array, with more than 99% of measured devices having the expected transfer characteristics considering the device dimensions. Since the as-grown SWCNTs used in this study consist of a mixture of metallic and semiconducting tubes with approximately one third having metallic properties, I_{ON}/I_{OFF} decreases as the channel length is decreased or the channel width increased and I_{ON}/I_{OFF} exceeding 10^3 is probable only when the length of the channel is approximately ten times the mean SWCNT length, or more than 40 μm. Due to their bottom-gate design, non-passivated channels and the use of SiO_2 as the gate dielectric, the devices exhibit large hysteresis that can be ascribed to trap states resulting from surface-bound water molecules in the vicinity of the SWCNTs[44-45], and in practice prevented by encapsulating the devices or switching to a top-gate design.

Out of 644 fabricated and measured devices, only one showed abnormal operation considering its channel dimensions, which could be ascribed to a defect in the substrate dielectric, leading to

substantial gate leakage, but unrelated to the deposition process. The best devices with dimensions $L_{CH} = W_{CH} = 100$ μm showed a charge carrier mobility exceeding 300 cm^2/Vs while simultaneously having a I_{ON}/I_{OFF} in excess of 10^6, and typical devices with $L_{CH} > 30$ μm showed charge carrier mobilities of 50-100 cm^2/Vs while simultaneously having I_{ON}/I_{OFF} ratios between 10^4-10^6. These represent some of the best metrics obtained for SWCNT TFTs fabricated from unsorted SWCNTs.

The average performance of the devices, as expressed by their I_{ON}, field effect device mobility and I_{ON}/I_{OFF} ratio, corresponded to or exceeded the performance of our earlier published devices[42] fabricated using SWCNTs from a similar process and a transfer method based on filter dissolution, amended with turbulent mixing of the aerosol to ensure uniform coverage on the filter. The comparison is even more favorable against earlier published TFTs[18] fabricated from aerosol-synthesized SWCNTs using filtration and filter dissolution without using a turbulent mixer[42] to ensure a uniform SWCNT coverage on the filter, the number of functional devices obtained here is an order of magnitude higher, underlining the uniformity of the deposited film. This is also supported by the lower spread in I_{ON}/I_{OFF} for devices with given channel dimensions obtained here.

From a practical point of view, thermophoretic deposition is in many ways preferable to transfer by filter dissolution, since the dissolution step is time-consuming and air bubbles trapped in the filter or agitation of the solvent during the dissolution, for example, may cause defects and non-uniformity in the transferred film. Based on atomic force microscopy (AFM, Veeco Dimension 5000 in intermittent contact (tapping) mode) of a finished device channel, the

SWCNT surfaces and channel remained free of any visible contamination. This is in contrast to devices fabricated using filter dissolution, where particulate remains, assumed to consist of insoluble parts of the nitrocellulose filter, could be observed even after extended soaking of the filter in acetone[42]. As we have concluded earlier[42], further improvements on the device properties would likely require either selective growth of semiconducting SWCNTs, preferably with a narrow diameter distribution, or post-growth removal of metallic SWCNTs.

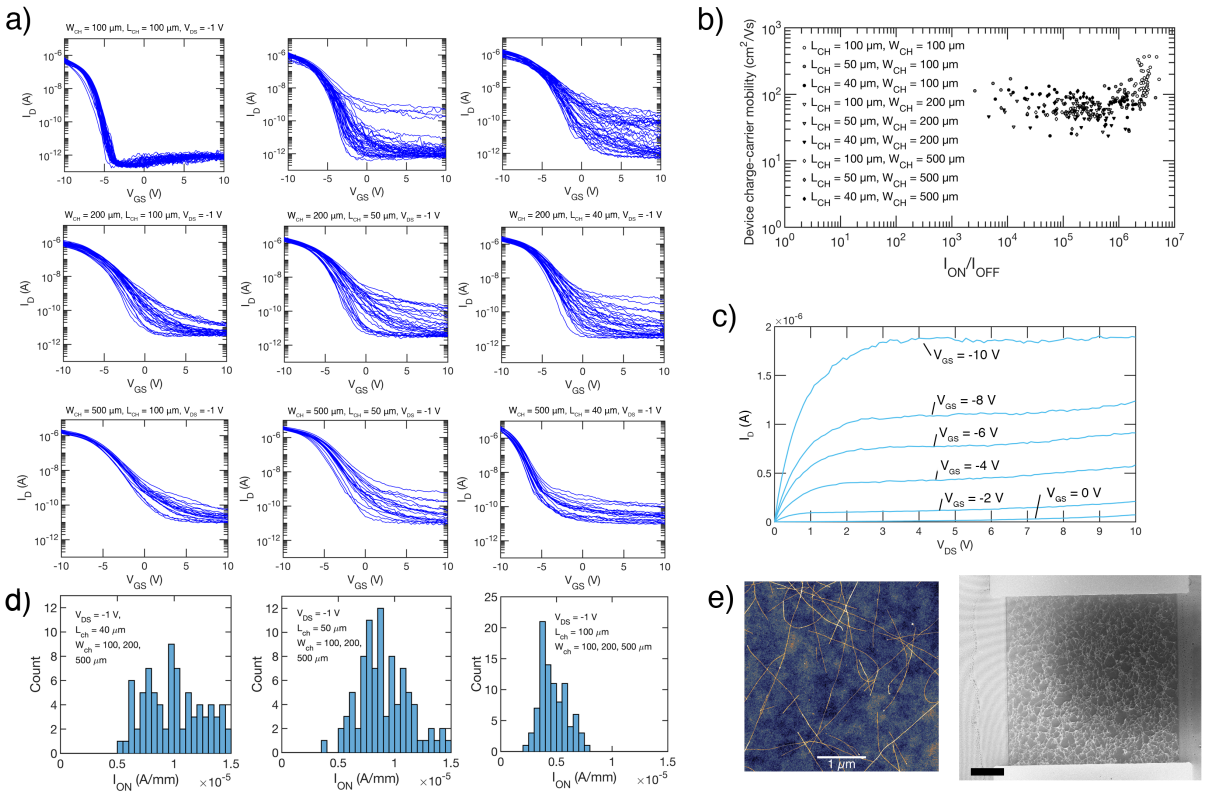

Figure 5. Electrical characterization and AFM and SEM micrographs of the fabricated TFTs. **a)** Transfer curves of devices with 100, 50 and 40 μm channel lengths and 500, 200 and 100 μm channel widths. **b)** Scatter plot for device mobility vs. I_{ON}/I_{OFF} ratios. **c)** Output curves of a representative L_{ch} = 50 μm, W_{ch} = 100 μm device. **d)** Histograms of I_{ON} (measured at V_{GS} = -10 V,

V_{DS} = -1 V and normalized to channel width) for devices with channel lengths 40, 50, and 100 μm. **e)** AFM (scale bar 1 μm) micrograph of SWCNTs in a finished device channel and SEM (scale bar 10 μm) micrograph of the entire channel.

Conclusions

Uniform, clean thin films of aerosol synthesized SWCNTs can be deposited on a centimeter scale even with a simple plate-to-plate precipitator design. The observed deposition rate of nanotubes is smaller than the classical prediction of Waldmann *et al*. and shows a slight dependence on the nanotube diameter. Based on this, we suggest the behavior is at least partially explained by the non-rigid body collisions between gas molecules and the nanometer-scale SWCNT surface. Partially aligned thin films can also be deposited by utilizing higher flow rates through the precipitator, at a cost of spatial uniformity in the simple laboratory-scale design considered here. Due to the simplicity of the method, it should be scalable up to wafer-scale or used in a geometry suitable for roll-to-roll processing with relative ease.

We have demonstrated the applicability of the method by controllably depositing near-percolating thin films of SWCNTs and utilizing them as TFT channels. The device performances and uniformity matched or exceeded previously published devices fabricated from similar SWCNTs using filter dissolution. In addition to the applications considered here, we suggest that the exceptionally clean, pristine SWCNTs deposited using the method could be deposited on low-dimensional solids for basic studies of their interactions, or utilized in the fabrication of optical and nanoelectromechanical devices and in the development of aerosol-based synthesis processes for SWCNTs.

Methods

SWCNT and Fe nano-agglomerate synthesis

SWCNTs were grown using the floating catalyst CVD process with ferrocene as the catalyst precursor and carbon monoxide (CO, 99%, Oy AGA AB, Finland) as the carbon feedstock. A detailed description of the SWCNT growth system has been published earlier[32]. To modulate the SWCNT mean diameter, a small (0.25 to 0.52 volume percent) flow of carbon dioxide (CO_2, 99.9993%, Oy AGA AB, Finland) was introduced to the reactor[46]. A total of three different growth conditions were used, with T = 850 ^{O}C and 0.25 vol-% CO_2 yielding SWCNTs with d = 1.2 nm, T = 850 ^{O}C and 0.4 vol-% CO_2 yielding SWCNTs with d = 1.5 nm, T = 850 ^{O}C and 0.52 vol-% CO_2 yielding SWCNTs with d = 1.9 nm. For brevity, these conditions and the SWCNTs are referred to by the mean diameter (*e.g.*, "1.2 nm SWCNTs"). The mean diameters of the SWCNTs were determined by UV/Vis/NIR absorbance spectroscopy (PerkinElmer LAMBDA 950 UV/Vis/NIR spectrophotometer, PerkinElmer Inc., United States) of press-transferred thin film samples and by comparing the positions of the absorption peaks corresponding to S_{11} and S_{22} electronic transitions with previously published empirical values[47].

The number size distribution at the outlet of the CVD reactor was determined by a scanning mobility particle sizer with condensation particle counter (SMPS+C system, GRIMM Aerosol Technik GmbH, Germany) consisting of a differential mobility analyzer (Vienna type DMA with electrode length 88 mm) and a condensation particle counter (Model 5414 CPC, cutoff size d_{50} = 4 nm) and was kept at or below $10^6/cm^3$ by adjusting the catalyst precursor feed to prevent excessive SWCNT agglomeration during growth[32].

Iron nanoparticle agglomerates were produced using a spark discharge generator (SDG). We have previously used the SDG as a catalyst source for SWCNT growth[28], using different

generator settings. Here, the particle size was increased, by increasing the discharge energy and decreasing the N_2 volume flow rate, to match the electrical mobility diameter of the SWCNTs and to reduce diffusive losses in the aerosol lines. The output of the spark discharge generator was mixed with additional filtered N_2 to obtain a total flow of 300 cm^3/min for deposition and to achieve a total flow of 1 l/min for measuring the number size distribution. The aerosol was passed through a vertical CVD furnace with a set temperature of 880°C for further agglomeration and sintering.

The number size distribution of the produced Fe nanoparticle agglomerates was measured using a SMPS+E system (scanning mobility particle sizer with electrometer, GRIMM Aerosol Technik GmbH, Germany) consisting of a differential mobility analyzer (Vienna type Nano-DMA, cutoff < 1 nm) and a Faraday cup electrometer (FCE, sensitivity of 0.1 fA).

Deposition efficiency measurements

The number concentration of aerosol passing through the thermophoretic precipitator was measured using a condensation particle counter (Model 5414 CPC, cutoff size d_{50} = 4 nm, GRIMM Aerosol Technik GmbH, Germany). A particle-free flow of laboratory air, filtered using an in-line HEPA filter cartridge (Balston DFU, Parker Hannifin Corp., United States) was used to match the CPC's volume flow rate of 300 cm^3/min when lower flow rates through the precipitator were used. The volume flow rates were measured using a primary flow calibrator (Gilian Gilibrator 2, Sensidyne, LP, United States). The temperatures of the TP plates were monitored using K-type thermocouples (Fluke Corp., United States) clamped to the plates. Both measurements were carried out with a logging interval of 10 seconds.

Thin film transistor fabrication

Device fabrication was carried out by removing SiO_2 from one side of Si/SiO_2 chips with 100 nm thermal oxide on both sides using buffered hydrofluoric acid, after which a common back-gate electrode (Al, 250 nm) was deposited on the bared doped Si by sputtering. Source and drain electrodes (Ti and Au, 5 and 40 nm) were patterned on the oxide using photolithography and electron beam evaporation, after which SWCNTs, synthesized at $850^{O}C$ with 0.25 vol.-% CO_2 (the d = 1.2 nm population) were deposited on the samples by the thermophoretic precipitator. SWCNTs outside the TFT channel areas were removed by covering the channels with photoresist (AZ 5214E, Microchemicals GmbH, Germany) and applying reactive ion etching using an O_2/Ar plasma. Before measuring the device properties, the photoresist was removed using commercial photoresist remover (AZ 100 Remover, Microchemicals GmbH, Germany) and the chips were washed in isopropyl alcohol and dried on a hot plate flushed with filtered dry nitrogen.

Supporting Information

Calculations of the thermophoretic terminal velocity based on the models of Li and Wang and Talbot *et al*., full sets of deposition efficiency measurements, TFT transfer curves for all characterized devices, an evaluation of the ON state resistance of devices as a function of the channel length, and micrographs of deposited SWCNTs on polymer substrates and prefabricated microstructures. This material is available free of charge *via* the Internet at http://pubs.acs.org.

Acknowledgements

The authors wish to thank Dr. Antti Kaskela for useful discussions regarding the depositor design and Akihiro Ishii and Dr. Yuichiro Kato (RIKEN, Japan) for providing the slotted

substrate for deposition. The research leading to these results has received funding from the European Union Seventh Framework Programme (FP7/2007-2013) under Grant Agreement Nos. 604472 (IRENA project) and the Aalto Energy Efficiency (AEF) Research Program through the MOPPI project. P.L. was partially supported by the Walter Ahlström Foundation and K.M. by the Finnish Foundations' Post Doc Pool. This work made use of the Aalto University Nanomicroscopy Center (Aalto-NMC) premises. Aalto NanoFab (Micronova) cleanroom resources are greatly appreciated.

REFERENCES

1. Wu, Z.; Chen, Z.; Du, X.; Logan, J. M.; Sippel, J.; Nikolou, M.; Kamaras, K.; Reynolds, J. R.; Tanner, D. B.; Hebard, A. F., Transparent, Conductive Carbon Nanotube Films. *Science* **2004,** *305* (5688), 1273-1276.
2. Snow, E.; Novak, J.; Campbell, P.; Park, D., Random Networks of Carbon Nanotubes as an Electronic Material. *Appl. Phys. Lett.* **2003,** *82* (13), 2145-2147.
3. Set, S. Y.; Yaguchi, H.; Tanaka, Y.; Jablonski, M.; Sakakibara, Y.; Rozhin, A.; Tokumoto, M.; Kataura, H.; Achiba, Y.; Kikuchi, K., Mode-Locked Fiber Lasers Based on a Saturable Absorber Incorporating Carbon Nanotubes. In *Optical Fiber Communication Conference*, Technical Digest (Optical Society of America, 2003), paper PD44.
4. Tans, S. J.; Verschueren, A. R.; Dekker, C., Room-Temperature Transistor Based on a Single Carbon Nanotube. *Nature* **1998,** *393* (6680), 49-52.
5. Kang, S. J.; Kocabas, C.; Ozel, T.; Shim, M.; Pimparkar, N.; Alam, M. A.; Rotkin, S. V.; Rogers, J. A., High-Performance Electronics Using Dense, Perfectly Aligned Arrays of Single-Walled Carbon Nanotubes. *Nat. Nanotechnol.* **2007,** *2* (4), 230-236.
6. Franklin, A. D.; Luisier, M.; Han, S.-J.; Tulevski, G.; Breslin, C. M.; Gignac, L.; Lundstrom, M. S.; Haensch, W., Sub-10 nm Carbon Nanotube Transistor. *Nano Lett.* **2012,** *12* (2), 758-762.
7. Desai, S. B.; Madhvapathy, S. R.; Sachid, A. B.; Llinas, J. P.; Wang, Q.; Ahn, G. H.; Pitner, G.; Kim, M. J.; Bokor, J.; Hu, C., MoS2 Transistors with 1-Nanometer Gate Lengths. *Science* **2016,** *354* (6308), 99-102.
8. Sazonova, V.; Yaish, Y.; Üstünel, H.; Roundy, D.; Arias, T. A.; McEuen, P. L., A Tunable Carbon Nanotube Electromechanical Oscillator. *Nature* **2004,** *431* (7006), 284-287.
9. Han, S.; Liu, X.; Zhou, C., Template-Free Directional Growth of Single-Walled Carbon Nanotubes on a-and r-Plane Sapphire. *J. Am. Chem. Soc.* **2005,** *127* (15), 5294-5295.
10. Patil, N.; Lin, A.; Myers, E. R.; Ryu, K.; Badmaev, A.; Zhou, C.; Wong, H.-S. P.; Mitra, S., Wafer-Scale Growth and Transfer of Aligned Single-Walled Carbon Nanotubes. *IEEE Trans. Nanotechnol.* **2009,** *8* (4), 498-504.

11. Sun, D. M.; Liu, C.; Ren, W. C.; Cheng, H. M., A Review of Carbon Nanotube-and Graphene-Based Flexible Thin-Film Transistors. *Small* **2013,** *9* (8), 1188-1205.
12. Zhou, Y.; Hu, L.; Grüner, G., A Method of Printing Carbon Nanotube Thin Films. *Appl. Phys. Lett.* **2006,** *88* (12), 123109.
13. Li, X.; Zhang, L.; Wang, X.; Shimoyama, I.; Sun, X.; Seo, W.-S.; Dai, H., Langmuir-Blodgett Assembly of Densely Aligned Single-Walled Carbon Nanotubes from Bulk Materials. *J. Am. Chem. Soc.* **2007,** *129* (16), 4890-4891.
14. Cao, Q.; Han, S.-j.; Tulevski, G. S.; Zhu, Y.; Lu, D. D.; Haensch, W., Arrays of Single-Walled Carbon Nanotubes with Full Surface Coverage for High-Performance Electronics. *Nat. Nanotechnol.* **2013,** *8* (3), 180-186.
15. Lu, K.; Lago, R.; Chen, Y.; Green, M.; Harris, P.; Tsang, S., Mechanical Damage of Carbon Nanotubes by Ultrasound. *Carbon* **1996,** *34* (6), 814-816.
16. Shelimov, K. B.; Esenaliev, R. O.; Rinzler, A. G.; Huffman, C. B.; Smalley, R. E., Purification of Single-Wall Carbon Nanotubes by Ultrasonically Assisted Filtration. *Chem. Phys. Lett.* **1998,** *282* (5), 429-434.
17. Kaskela, A.; Nasibulin, A. G.; Timmermans, M. Y.; Aitchison, B.; Papadimitratos, A.; Tian, Y.; Zhu, Z.; Jiang, H.; Brown, D. P.; Zakhidov, A.; Kauppinen, E. I., Aerosol-Synthesized Swcnt Networks with Tunable Conductivity and Transparency by a Dry Transfer Technique. *Nano Lett.* **2010,** *10* (11), 4349-4355.
18. Sun, D.; Timmermans, M. Y.; Tian, Y.; Nasibulin, A. G.; Kauppinen, E. I.; Kishimoto, S.; Mizutani, T.; Ohno, Y., Flexible High-Performance Carbon Nanotube Integrated Circuits. *Nat. Nanotechnol.* **2011,** *6*, 156-161.
19. Mädler, L.; Roessler, A.; Pratsinis, S. E.; Sahm, T.; Gurlo, A.; Barsan, N.; Weimar, U., Direct Formation of Highly Porous Gas-Sensing Films by in situ Thermophoretic Deposition of Flame-Made Pt/SnO2 Nanoparticles. *Sens. Actuators, B* **2006,** *114* (1), 283-295.
20. Gonzalez, D.; Nasibulin, A. G.; Baklanov, A. M.; Shandakov, S. D.; Brown, D. P.; Queipo, P.; Kauppinen, E. I., A New Thermophoretic Precipitator for Collection of Nanometer-Sized Aerosol Particles. *Aerosol Sci. Technol.* **2005,** *39*, 1064-1071.
21. Na, H.; Park, J. H.; Hwang, J.; Kim, J., Site-Specific Growth and Density Control of Carbon Nanotubes by Direct Deposition of Catalytic Nanoparticles Generated by Spark Discharge. *Nanoscale Res. Lett.* **2013,** *8*, 409.
22. Waldmann, L.; Schmitt, K. H., Thermophoresis and Diffusiophoresis of Aerosols. In *Aerosol Science*, Davies, C. N., Ed. Academic Press Inc.: London, 1966; pp 137-162.
23. Mädler, L.; Friedlander, S. K., Transport of Nanoparticles in Gases: Overview and Recent Advances. *Aerosol and Air Quality Research* **2007,** *7* (3), 304-342.
24. Bird, R. B.; Stewart, W. E.; Lightfoot, E. N., *Transport Phenomena*. John Wiley & Sons: New York, 2002.
25. Friedlander, S. K., *Smoke, Dust and Haze: Fundamentals of Aerosol Dynamics, 2nd Ed.* Oxford University Press: New York, 2000.
26. Rosner, D. E.; Mackowski, D. W.; Garcia-Ybarra, P., Size- and Structure-Lnsensitivity of the Thermophoretic Transport of Aggregated "Soot" Particles in Gases. *Combust. Sci. Technol.* **1991,** *80*, 87-101.
27. Zurita-Gotor, M., Size- and Structure-Independence of the Thermophoretic Transport of an Aerosol Particle for Specular Boundary Conditions in the Free Molecule Regime. *J. Aerosol Sci.* **2006,** *3* (37), 283-291.

28. Mustonen, K.; Laiho, P.; Kaskela, A.; Zhu, Z.; Reynaud, O.; Houbenov, N.; Tian, Y.; Susi, T.; Jiang, H.; Nasibulin, A. G.; Kauppinen, E. I., Gas Phase Synthesis of Non-Bundled, Small Diameter Single-Walled Carbon Nanotubes with Near-Armchair Chiralities. *Appl. Phys. Lett.* **2015,** *107*, 013106.
29. Moisala, A.; Nasibulin, A. G.; Shandakov, S. D.; Jiang, H.; Kauppinen, E. I., On-Line Detection of Single-Walled Carbon Nanotube Formation During Aerosol Synthesis Methods. *Carbon* **2005,** *43* (10), 2066-2074.
30. Mustonen, K.; Laiho, P.; Kaskela, A.; Susi, T.; Nasibulin, A. G.; Kauppinen, E. I., Uncovering the Ultimate Performance of Single-Walled Carbon Nanotube Films as Transparent Conductors. *Appl. Phys. Lett.* **2015,** *107*, 143113.
31. Jariwala, D.; Marks, T. J.; Hersam, M. C., Mixed-Dimensional Van der Waals Heterostructures. *Nature Materials* **2016**.
32. Kaskela, A.; Laiho, P.; Fukaya, N.; Mustonen, K.; Susi, T.; Jiang, H.; Houbenov, N.; Ohno, Y.; Kauppinen, E. I., Highly Individual SWCNTs for High Performance Thin Film Electronics. *Carbon* **2016,** *103* (228-234).
33. Company, C. *Flow of Fluids through Valves, Fittings and Pipe. Technical Paper No. 410*; 1988.
34. Haynes, W. M., *Crc Handbook of Chemistry and Physics*. 96 ed.; CRC Press: Boca Raton, Florida, 2015.
35. Li, Z.; Wang, H., Drag Force, Diffusion Coefficient, and Electric Mobility of Small Particles. II. Application. *Phys. Rev. E* **2003,** *68*, 061207.
36. Li, Z.; Wang, H., Thermophoretic Force and Velocity of Nanoparticles in the Free Molecule Regime. *Phys. Rev. E* **2004,** *70*, 021205
37. Wang, J.; Luo, S.; Xia, G., Thermophoretic Force on Nanocylinders in the Free Molecule Regime. *Phys. Rev. E* **2017,** *95* (3), 033101.
38. Pop, E.; Mann, D.; Wang, Q.; Goodson, K.; Dai, H., Thermal Conductance of an Individual Single-Wall Carbon Nanotube above Room Temperature. *Nano Lett.* **2006,** *6* (1), 96-100.
39. Talbot, L.; Cheng, R.; Schefer, R.; Willis, D., Thermophoresis of Particles in a Heated Boundary Layer. *J. Fluid Mech.* **1980,** *101* (04), 737-758.
40. Tsai, C.-J.; Lin, J.-S.; Aggarwal, S. G.; Chen, D.-R., Thermophoretic Deposition of Particles in Laminar and Turbulent Tube Flows. *Aerosol Sci. Technol.* **2004,** *38* (2), 131-139.
41. Usov, I.; Mezzenga, R., FiberApp: An Open-Source Software for Tracking and Analyzing Polymers, Filaments, Biomacromolecules, and Fibrous Objects. *Macromolecules* **2015,** *48* (5), 1269-1280.
42. Kaskela, A.; Mustonen, K.; Laiho, P.; Ohno, Y.; Kauppinen, E. I., Toward the Limits of Uniformity of Mixed Metallicity Swcnt TFT Arrays with Spark-Synthesized and Surface-Density-Controlled Nanotube Networks. *ACS Appl. Mater. Interfaces* **2015,** *7*, 28134-28141.
43. Cao, Q.; Xia, M.; Kocabas, C.; Shim, M.; Rogers, J. A.; Rotkin, S. V., Gate Capacitance Coupling of Singled-Walled Carbon Nanotube Thin-Film Transistors. *Appl. Phys. Lett.* **2007,** *90*, 023516.
44. Kim, W.; Javey, A.; Vermesh, O.; Wang, Q.; Li, Y.; Dai, H., Hysteresis Caused by Water Molecules in Carbon Nanotube Field-Effect Transistors. *Nano Lett.* **2003,** *3* (2), 193-198.
45. Pascal-Levy, Y.; Shifman, E.; Pal-Chowdhury, M.; Kalifa, I.; Rabkin, T.; Shtempluck, O.; Razin, A.; Kochetkov, V.; Yaish, Y., Water-Assisted Mobile Charge Induced Screening and

Origin of Hysteresis in Carbon Nanotube Field-Effect Transistors. *Phys. Rev. B* **2012,** *86* (11), 115444.
46. Tian, Y.; Zavodchikova, M.; Kivistö, S.; Nasibulin, A. G.; Zhu, Z.; Jiang, H.; Okhotnikov, O. G.; Kauppinen, E. I., Tailoring the Diameters of Single-Walled Carbon Nanotubes for Optical Applications. *Nano Res.* **2011,** *4*, 807-815.
47. Weisman, R. B.; Bachilo, S. M., Dependence of Optical Transition Energies on Structure for Single-Walled Carbon Nanotubes in Aqueous Suspension: An Empirical Kataura Plot. *Nano Lett.* **2003,** *3* (9), 1235–1238.

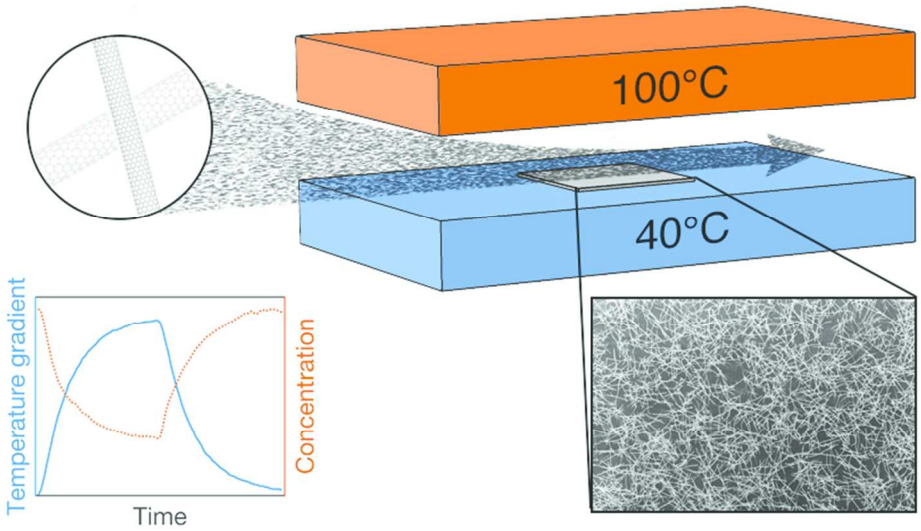

Table of Contents graphic for manuscript

74x39mm (300 x 300 DPI)